Interrogation and control of condensed phase chemical dynamics with linearly chirped pulses: I_2 in solid Kr

M. Sterling, R. Zadoyan, and V. A. Apkarian
Department of Chemistry, University of California, Irvine, California 92717

(Received 19 October 1995; accepted 30 January 1996)

The effect of linearly chirped pulses in condensed phase ultrafast pump–probe experiments is investigated by classical simulations for the model system of I_2 isolated in a Kr matrix. The central frequency of the probe laser is selected to monitor exclusively the event of first collision and recoil of atoms from the host cage. It is shown that a chirped probe pulse enables characterization of the magnitude and sign of the momentum of the evolving trajectory flux. This can be understood by transforming the frequency–time profile of the probe pulse to coordinate–time space, and noting that the observable signal is a function of the relative group velocities of the traveling wave packet and the traveling window function. The effect of the pump pulse chirp, is a measure of the controllability of the evolving dynamics. In the particular case studied, breaking and remaking of the I_2 bond near the dissociation limit of the bare molecule, it is shown that the memory of the system outlasts the collision with the cage. Negatively chirped pulses produce a more tightly focused wave packet during recoil, leading to a stronger population coherence in the subsequent dynamics. [S0021-9606(96)02317-2]

INTRODUCTION

The availability of lasers with ultrashort pulses naturally raises the question of affecting chemistry by sculpted radiation fields. Laser control of chemical dynamics is accordingly an active field of research both in theory and experiment. We only cite a sampling of this burgeoning literature.[1–14] The simplest sculpting of an optical pulse would be the shaping of its time–frequency profile, namely the chirp of the pulse.[15] Theoretically optimized chirped pulses have already been used to experimentally demonstrate coherent control of wavepackets in one dimensional systems, namely diatomics in the gas phase, and I_2 in particular.[14] In systems of low dimensionality, the concept can be tested by nearly exact theoretical analysis of the matter-radiation Hamiltonian.[1–6] In contrast, in multidimensional systems, as in the case of condensed media where many-body interactions govern the evolving dynamics, the approximations required for analysis of even the simplest thought experiments are severe and their validity is difficult to assess. Experimental reality in such cases is indispensable. To this end, model systems which can be scrutinized by experiment and theory are quite useful. Molecular iodine isolated in cryogenic rare gas matrices represents such a model system. Recent studies of this system by ultrafast pump–probe experiments have produced a rather detailed picture of the breaking and remaking of the iodine bond in the constrained environment of the matrix cage.[16–18] The extant level of detail with which this system is understood, is sufficient to enable us to test the effects of chirped pulses on the preparation of the system and its dynamical observables—the pump pulse and the probe pulse. We provide here a theoretical analysis of a particular case study, which is inspired by preliminary experiments.[19]

I_2 isolated in solid Kr is the system under consideration. Upon dissociative excitation of the molecule to the $A(^3\Pi_{1u})$ state with a short laser pulse, the evolving dynamics is monitored by laser induced fluorescence with a second short laser pulse which promotes the molecule to the $\beta(1_g)$ ion-pair state.[20] Although initially excited above the dissociation limit of the bare molecule, the lattice cage prevents permanent dissociation. The ''cage effect'' is complete, i.e., recombination proceeds within the cage with unit probability. In the present, the experimental conditions are chosen to isolate only the single event of caging for observation. This is achieved by choosing a probe wavelength near the minimum of the $\beta-A$ difference potential, near 400 nm, which limits the observation window to view the outward stretch of the molecule prior to collision with the cage, and the postcollision recoil of the atoms from the cage. This enables a direct and detailed analysis of the primary process which controls subsequent coherences in the system. The controllability of this step would determine the controllability of all subsequent dynamics. We will consider a pump wavelength near 800 nm, which would prepare the molecule near its gas phase dissociation limit. The choice of this excitation energy is deliberate. It is motivated by experimental convenience: the fundamental output of a Ti:sapphire laser can be used as the pump source, and its first harmonic can be used as the probe source.

Despite the limited scope of the study to be reported, the vectorial character of information obtained by probing with chirped pulses can be most generally deduced, and it can clearly be concluded that at least in the particular case study, coherent control of the many-body dynamics is possible.

In the analysis to be given below, we closely follow the methods and approximations implemented in the prior treatments of this system, which had produced a close agreement between experiment and simulation.[16–18] We rely on classical mechanics for simulation of the many-body dynamics, and we rely on the classical Franck principle for the simulation of the pump–probe observables.[21] Given the fact that the

TABLE I. Potential parameters.

	Form	Parameters
Kr–Kr	Lennard-Jones	ϵ=199.9 K, σ=3.58 Å
I–Kr	Lennard-Jones	ϵ=233.5 K, σ=3.74 Å
I_2 (X)	Morse	D_e=12 550 cm^{-1}, β=1.871 Å^{-1}, r_e=2.65 Å
I_2 (A)	Morse	D_e=1887 cm^{-1}, β=2.1 Å^{-1}, r_e=3.10 Å
I^+I^-	Rittner[a]	a=7.218 14×10^4 cm^{-1}, b=1.846×10^7 cm^{-1}, β=2.1426 Å^{-1}, c_1=1.161 41×10^5 cm^{-1}, c_3=−8.3×10^4 cm^{-1}, c_4=9.0×10^5 cm^{-1}, c_6=1.4×10^6 cm^{-1}, Δa=3600 cm^{-1}, $R=r-0.2$ Å

[a]Rittner form used, $V=(a-\Delta a)+b[\exp(-\beta R)]-(c_1/R)+(c_3/R^3)-(c_4/R^4)-(c_6/R^6)$.

dynamics under consideration involves many heavy atoms, it is not surprising that classical mechanics represents an adequate description of the relevant equations of motion. Moreover, in the narrow energy range of preparation on the $I_2(A)$ surface, it has already been demonstrated that the dynamics is strictly adiabatic, evolving on a single electronic surface.[18] The classical Franck principle,[21] or the reflection approximation,[22] which is commonly used in gas phase bound-to-free transitions, is more broadly applicable in condensed media where absorption spectra are broadened due to electronic dephasing, due to coupling of the chromophore mode with those of the bath.[23] The condition for the validity of this treatment can be more precisely stated in the time dependent view of optical transitions, the Heisenberg representation, in which the absorption spectrum is given as the Fourier transform of the auto correlation of the ground state wavefunction evolving on the excited state potential.[24,25] As the correlation window becomes shorter than dynamical recursions, either due to using ultrafast lasers or due to fast dephasing of the multidimensional wave function, the classical approximation becomes nearly exact for a correlation window limited to times shorter than the first recursion in the correlation function. This limit in pump–probe experiments has been referred to as the ''snapshot limit,''[26] and represents a good approximation for the system under consideration here, particularly since we are not concerned with any overlap in time between pump and probe lasers. The main quantum effect that needs to be accounted in these treatments is the zero point energy of the lattice, which at cryogenic temperatures governs the phase space distribution sampled by the pump pulse, which in turn governs the extent of coherence in the subsequent dynamics.[17] Thus, the sampling of initial conditions of the trajectories requires some care. We rely on temperature scaling to mimic the quantum distribution by the classical simulations.[27,17,18]

SIMULATIONS

Although the present simulations closely follow those previously implemented for this system, we reiterate the method, specifically noting the approximations made. A single I_2 molecule, isolated in a double-substitutional site of a fcc lattice of Kr is used. The infinite solid is approximated by using a simulation cell of 500 Kr atoms, subject to periodic boundary conditions. Pairwise additive atom–atom potentials are used for all interactions. Lennard-Jones potentials are used to describe both Kr–Kr and I–Kr interactions. For the latter pair, parameters appropriate for Xe–Kr are used (see Table I). The system is thermalized on the $I_2(X)$ surface, while the dynamics is propagated on the $I_2(A)$ surface. The initial sampling of configurations is accomplished by selecting configurations from a thermalization run, subject to the condition that the vertical $A \leftarrow X$ excitation correspond to the pump laser profile. Since in these simulations the I–Kr interaction is assumed to be independent of the electronic state of I_2, a given I–I distance corresponds to a unique excitation energy. Accordingly, the sampling for a given pump laser profile reduces to sampling of a proper initial distribution of I_2 bond lengths. The distribution of initial bond lengths, $P(r_0)$, is obtained from the power spectrum of the pump laser, $P(\hbar\omega)$, by equating $\hbar\omega$ to the difference potential, $\Delta V(r)$, between the A and X states,

$$P(r_0)dr=\int P(\hbar\omega)\delta[\hbar\omega-\Delta V(r)]d\hbar\omega, \tag{1}$$

yielding

$$P(r_0)=P[\Delta V(r)]|\partial\Delta V(r)/\partial r|. \tag{2}$$

This is the statement of the classical reflection approximation, which is equivalent to the classical Franck principle for optical transitions, and will be revisited in the simulation of the spectra. In the limited range of interest, the difference potential can be well fitted by an exponential; then for a Gaussian laser pulse profile, a log normal distribution of bond lengths is required. We will rely on an ensemble of 120 trajectories, with an initial distribution of I_2 bond lengths given by Eq. (2), using a Gaussian laser intensity profile of 120 cm^{-1} FWHM, corresponding to a transform limited pump pulse width of 120 fs. The lattice configurations correspond to realizations of the thermalized microcanonical ensemble, which is generated by propagating the molecular dynamics on the X state, at an artificially scaled temperature of 45 K, to account for the zero-point amplitudes of the lattice.[17]

Given the initial sampling of configurations, the classical trajectories are propagated on the single potential energy surface of $I_2(A)$ by standard methods.[28] To simulate the observable signal, the time dependent probe transition which promotes the molecule to the ion-pair states, has to be modeled. Polarization measurements show that the probe transition di-

pole is parallel to the molecular axis both in absorption and emission, maintaining the $\Delta\Omega=0$ propensity established in the gas phase for these covalent to ionic transitions.[29] Accordingly, the absorption can be identified as $I_2(\beta \leftarrow A)$. Here, also, we make the approximation that the I–Kr interactions in the ion-pair and covalent state are identical. This assumption allows the modeling of the probe absorption by a one-dimensional spectral inversion, using the electronically solvated ion-pair potential. While, *a priori*, the validity of this approximation is not obvious, its success has implications about the nature of the vertically accessed states which are discussed elsewhere.[30] In the present, we suffice by the justification that in the prior treatments the approximation has proved to be quite satisfactory.[16–18,31] For the solvated ion-pair potential we use the Rittner form which describes these states in the gas phase, after adjustments made to reproduce the transient resonances in the prior studies; a vertical solvation of 3600 cm^{-1} and a shift of the potential to larger R by 0.2 Å (see Table I). In this one-dimensional approximation, the probe pulse spectral distribution can be mapped along $r(I_2)$ by the same transformation used in Eq. (2), i.e., by reflection from the difference potential. This defines the probe window, $W(r)$. We consider a transform limited Gaussian probe pulse width of FWHM=41 fs, which corresponds to a Gaussian spectral distribution of FWHM=350 cm^{-1}. Since the difference potential is double valued, for a given central wavelength two configurations are probed simultaneously, except at the minimum of the difference potential, where the two windows degenerate into one. Thus, for illustration purposes, we will consider probe pulses centered at two different wavelengths, at 393 nm and 398 nm, both of which lie within the doubled $Ti:Al_2O_3$ laser bandwidth. The time dependent pump–probe signal, in the relevant weak field limit, can then be obtained by separate convolutions of the trajectory ensemble with the time profiles of the pump and probe windows, $P(r_0,t)$ and $W(r,t)$, respectively. These transformations have a significant bearing on the observables, accordingly we discuss them explicitly considering three cases from which all other possibilities can be deduced. In what follows, we will refer to the Wigner distribution of the laser in the frequency–time domain as the pulse profile,[15] and we will refer to its projection in coordinate–time domain as the window profile.

RESULTS AND DISCUSSION

Case (a): Unchirped pump and unchirped probe

Since the time ordering of the trajectories in this case is random, there is no causality, hence the order of time convolutions is immaterial. The double convolution with the pump and probe pulses is then more conveniently evaluated as a single convolution of the trajectory ensemble with the temporal cross-correlation between pump and probe. Defining the evolving population density, $\rho(R,t)$, by the trajectory ensemble of the I_2 bond lengths as a function of time,

$$\rho(t,R;R_0)\equiv\{R_i(t)\}. \tag{3}$$

And the time dependent pump and probe window functions as products of spatial and temporal distributions,

$$P(r_0,t)\equiv P(r_0)P(t), \tag{4a}$$

$$W(r,t)\equiv W(r)W(t). \tag{4b}$$

Using the temporal cross correlation between pump and probe laser windows,

$$W'(t)=\int_{-\infty}^{\infty}P(\tau)W(t+\tau)d\tau, \tag{5}$$

the pump–probe signal, i.e., excitation of population reaching the probe window after a time t from initial preparation with the pump laser, is generated as

$$S(t)=\int_{-\infty}^{\infty}\sum_i W[R_i(\tau)]W'(t-\tau)d\tau. \tag{6}$$

The explicit notation of R_0 is dropped in Eq. (6) for the sake of brevity, and since the index i clearly assigns R to a unique trajectory starting at R_0. The usual assumption is a Gaussian time profile for the unchirped pulses, with a cross correlation width that is either measured initially or obtained directly from the experiment where response limited transients are present. The above procedure is in effect the method used in the prior simulations of pump–probe signals, except that there, instead of explicitly considering the window function via the reflection approximation, in effect, a Gaussian spatial profile was assumed.[18]

In Fig. 1 we illustrate the procedure outlined above for probing at 398 nm, where the two windows collapse into one. We show the pulse profile of a 41 fs transform limited probe laser, and the window function resulting from its projection on the $r-t$ plane, after convolution of this function with the pump pulse, to yield $W(r)W'(t)$, i.e., a window function which maintains the spatial distribution of the probe window but is broadened in time to represent the pump–probe cross correlation width. This function is then convoluted with the trajectory ensemble, which is represented by five of its members in Fig. 1(b). The resulting signal, which is also illustrated, can be understood as the integral under the window which is advanced in time in the $r-t$ plane. The signal is composed of two peaks representing two dynamical resonances. The first is the precollision resonance, which captures the wave packet on its outbound stretch, just before colliding with the cage wall. The second is the postcollision resonance, which captures the recoiling wave packet after collision with the cage. The width of the first peak is response limited, it represents the cross-correlation width of the pump and probe pulses. After the collision, the packet spreads in phase space, and now the width of the signal accurately measures the dispersion of the trajectories. *The integrated area of a given signal peak is inversely proportional to the instantaneous group velocity of the packet*. This has been noted previously, and can be shown analytically for an assumed form of a wave packet. Thus if we assume a traveling Gaussian wave packet for the trajectory ensemble,

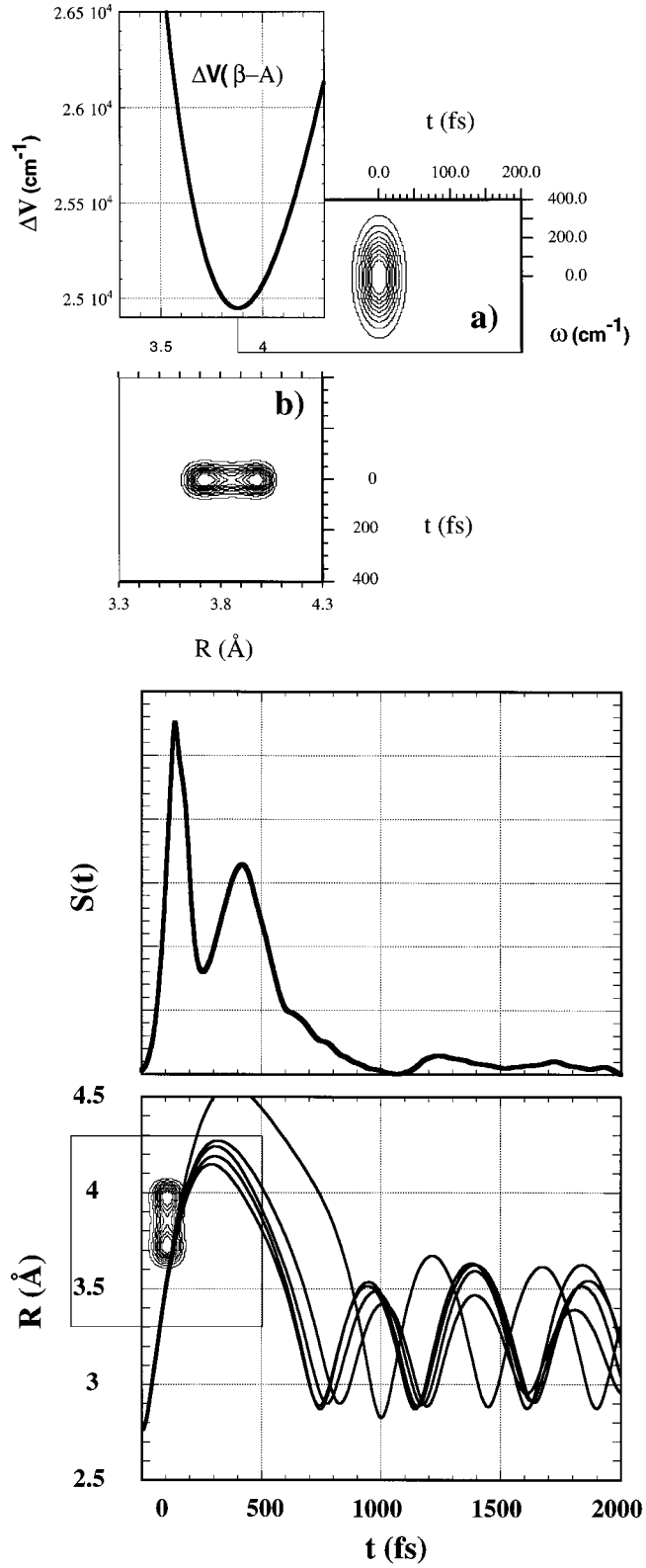

FIG. 1. (Above) Transformation of the 398 nm probe pulse from the ω–t plane, to the r–t plane. The profile of a transform limited pulse, FWHM=41 fs with a center wavelength of 398 nm is shown in (a). Using the difference potential ΔV between the ion-pair and A state, the pulse is transformed to the r–t plane. The profile in (b) corresponds to $W(r)W'(t)$, i.e., the window function after convolution with the pump-pulse of FWHM =120 fs. (Below) The trajectory ensemble is represented by five of its members in the lower panel, the probe window function is also shown on the same scale. The simulated signal, $S(t)$, is shown in the top panel.

$$\rho(r,t) \equiv \exp\left[-\frac{(r-vt)^2}{\delta^2}\right] \tag{7}$$

and a probe window function,

$$W(r,t,\tau) \equiv \delta(r-r^*)\exp\left[-\frac{(t-\tau)^2}{\Delta^2}\right], \tag{8}$$

where τ is the delay between the pump and probe pulses, and in which for convenience, but without loss of generality, we assume a delta function for the spatial distribution of the window. The integrated area of the signal can be obtained using standard Gaussian integrals,

$$\begin{aligned}\int S(\tau)d\tau &= \int_{-\infty}^{\infty} d\tau \int_{-\infty}^{\infty} dt \int_{-\infty}^{\infty} dr\rho(r,t)W(r,t,\tau)\\ &= \frac{1}{v}\int_{-\infty}^{\infty} d\tau \int_{-\infty}^{\infty} d(vt)\exp\left[-\frac{(vt-r^*)^2}{\delta^2} - \frac{(vt-v\tau)^2}{v^2\Delta^2}\right]\\ &= \delta\Delta\sqrt{\frac{\pi}{\delta^2+v^2\Delta^2}}\int_{-\infty}^{\infty} d\tau \times \exp\left[-\frac{(r^*-v\tau)^2}{\delta^2+v^2\Delta^2}\right]\\ &= \frac{\pi\delta\Delta}{v}.\end{aligned} \tag{9}$$

This is strictly valid for well resolved signal peaks, which represent a single crossing of the entire packet through the window. We also note that in the case of an unchirped pulse since the window profile is separable into independent r and t distributions, Eq. (4a), integration over a window function other than the delta function used above does not change the result of Eq. (9). For an arbitrary wave packet with a defined group velocity, we can generalize that *the integrated intensity under a resonance that corresponds to a single crossing of the probe window is inversely proportional to the group velocity of the packet.* In the present case, a ratio of areas between the precollision resonance and the postcollision resonance of 1:2 agrees well with the ensemble averaged velocity ratio of the trajectories of 2:1 under these windows. In effect, 50% of the momentum of the dissociating molecule is imparted to the lattice.

Figure 2 illustrates the simulation of the signal for a probe pulse centered at 393 nm, where the window splits into an inner and outer resonance. The signal in this case can be regarded as the sum of contributions from each of the windows. Since the trajectories now cross the windows at four different times, twice in the outgoing wave and twice during rebound. With short pump and probe pulses the group velocity of the wave packet can be clocked rather accurately in this case.

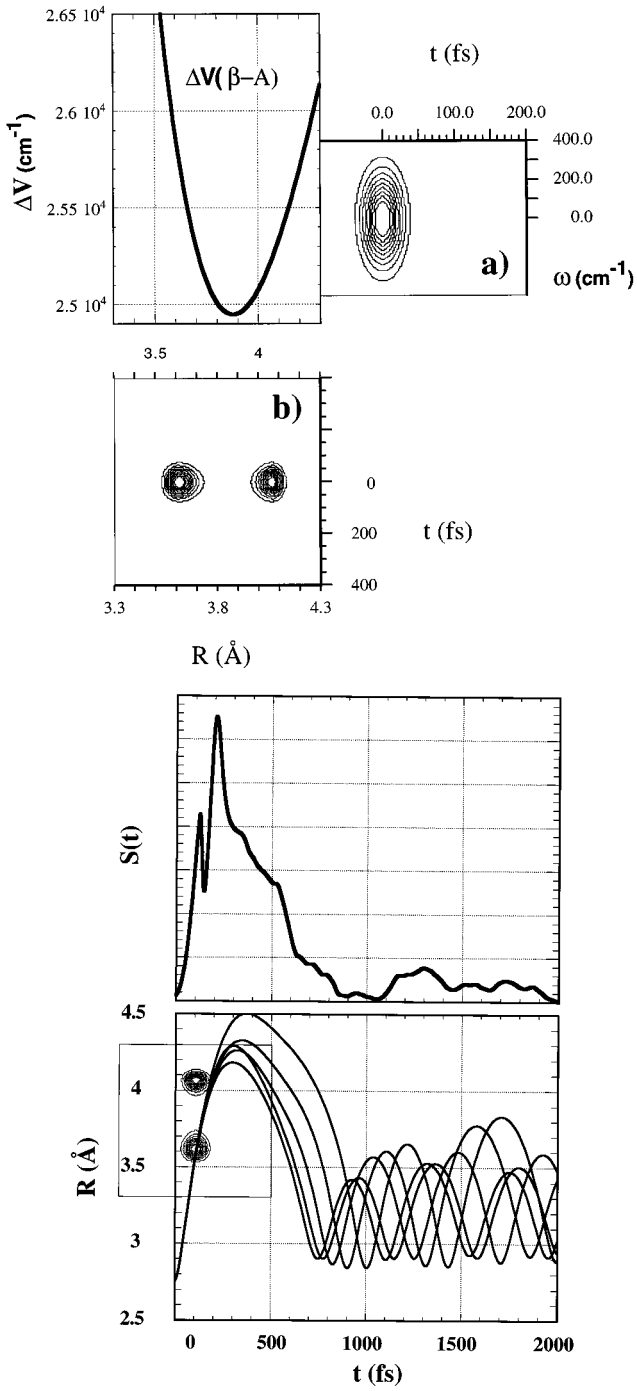

FIG. 2. (Above) Same as in Fig. 1(a), except for a probe pulse centered at 393 nm. In this case, the window function splits into two, due to the double valued nature of the difference potential. (Below) (Lower panel) Representative members of the trajectory ensemble, and the probe window function. (Upper panel) Simulated signal. The first two spikes in the signal correspond to passage of the outbound trajectories through the inner and outer window, the two broader shoulders at later time correspond to passage of the recoiling trajectories through the same two windows.

Case (b): Unchirped pump, linearly chirped probe

A linearly chirped pulse is constructed from a transform limited pulse by linear transformation of the time axis, $t \rightarrow t \pm \alpha\omega$, where α is the slope of the time vs frequency profile of the pulse,

$$I(\omega,t)=\exp\left[-\left(\frac{(\omega-\omega_0)^2}{2(\Delta\omega)^2}+\frac{\{t-[t_0\pm\alpha(\omega-\omega_0)]\}^2}{2(\Delta t)^2}\right)\right]. \tag{10}$$

This can be projected unto the coordinate space, using the resonance condition $\hbar\omega=\Delta V(r)$ as in Eq. (2), to obtain the window function,

$$W(r,t)=\exp\left\{-\left[\frac{[\Delta V(r)-\omega_0]^2}{2(\Delta\omega)^2}+\frac{(t-\{t_0\pm\alpha[\Delta V(r)-\omega_0]\})^2}{2(\Delta t)^2}\right]\right\}\left|\frac{\partial\Delta V(r)}{\partial r}\right|. \tag{11}$$

Note, the classical reflection approximation fails at the extreme of the difference potential where the differential element in Eq. (11) leads to singularities. In such cases, the window function should be uniformized by treating it as an expectation value over the minimum uncertainty spread in position.[16–18] This consideration arises in the present in the case of the 398 nm resonance, where the minimum of the difference potential lies within the spectral distribution of the probe laser. Instead of first smoothing the window function by using the zero-point amplitude distribution of the ion-pair state, since $\hbar\Delta(\omega)\leqslant\langle\partial\Delta V/\partial r\rangle\langle\Delta r\rangle$ it is more convenient to simply ignore the differential element in Eq. (11) and to allow the time convolutions of the window with the swarm to produce the desired averaging process. These considerations do not arise in the case of the 393 nm resonance which is sufficiently removed from the minimum of the difference potential.

The transformations of a negatively chirped pulse at the two probe wavelengths considered are illustrated in Fig. 3. The full expression of Eq. (11) is used in the case of the 393 nm resonance, while the differential element is dropped in the case of the 398 nm resonance. In each case, the assumed value of $\alpha=0.2$ fs/cm^{-1}, broadens the time profile of the pulse by nearly a factor of 2. The mapping of the pulse on the $r-t$ plane is useful for understanding the effect of chirp on the observable signal. Note that although the pulse is chirped linearly in time, the transformation of the spectral distribution via the difference potential distorts the window profile. In the case of the 398 nm resonance, the mapping in coordinate space approximates a quadratic chirp of r vs t, reflecting the quadratic nature of the difference potential at this resonance. At 393 nm, the two window functions approximate linear chirps, however with opposite signs, reflecting the fact that they result from regions of the difference potential that can be approximated by linear but opposite slopes.

The signal in this case is generated by first convoluting the trajectory ensemble with the chirped probe window function, and subsequently convoluting with the temporal profile of the pump pulse,

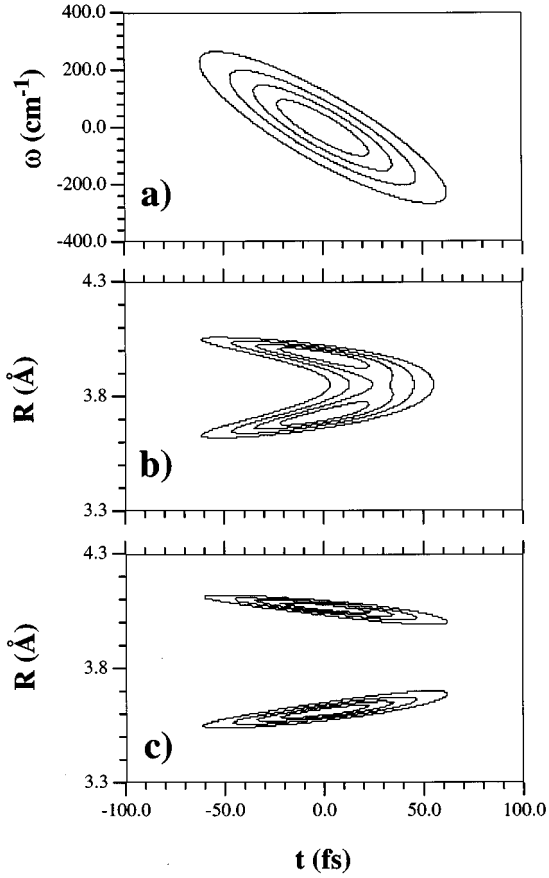

FIG. 3. Transformations of a negatively chirped pulse from ω–t to $r-t$ planes. (a) A negatively chirped pulse of FWHM=41 fs, and a chirp slope α=0.202 fs/cm^{-1} in the ω–t plane; (b) the projection of the same pulse in the $r-t$ plane via the difference potential shown in Fig. 1(a), and assuming a central wavelength of 398 nm; (c) same as in (b) but for a central wavelength of 393 nm. The $r-t$ projections do not include the differential term [see Eq. (11)].

$$S(t)=\int_{-\infty}^{\infty} d\tau' P(t-\tau') \int_{-\infty}^{\infty} d\tau \times \sum_i \exp\left\{ -\left[\frac{\{\Delta V[R_i(\tau)]-\omega_0\}^2}{2(\Delta\omega)^2} + \frac{(\tau'-\tau\pm\alpha\{\Delta V[R_i(\tau)]-\omega_0\})^2}{2(\Delta t)^2} \right] \right\} \left| \frac{\partial \Delta V}{\partial r} \right|_{R_i}. \tag{12}$$

The convolution with the pump pulse simply broadens the response function. The effect of the probe chirp is the more interesting. The slope of a trajectory in the $r-t$ plot clearly corresponds to velocity. Averaged over the trajectory ensemble, it yields the group velocity of the wave packet. In the same fashion, the slope of a linearly chirped window function in the $r-t$ plane corresponds to the group velocity of the traveling window. The relative velocities of the window function and the trajectory ensemble determine the signal shape; where the window and trajectories are counterpropagating, a narrower, and accordingly sharper peak in the signal will appear, while the opposite will occur where the two propagate in the same direction. In the specific case considered here, since both the stretch and compression of the I–I bond are monitored, the effect of a linearly chirped pulse in the $r-t$ plane is to change the relative heights of these two resonances.

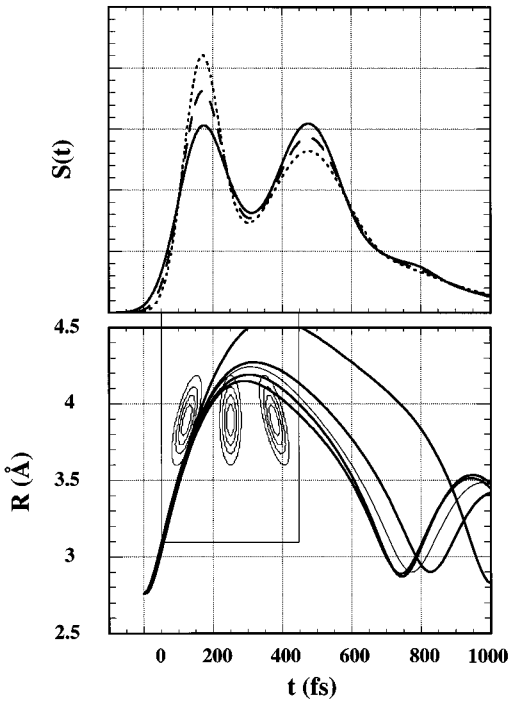

FIG. 4. The effect of probing with chirped pulses. The observable signal for positively (solid line), negatively (dotted line), and unchirped (dashed line) window functions is shown in the top panel. Representative members of the trajectory ensemble, along with the window functions are shown in the lower panel. Where the slopes of the trajectories and the window function have the same sign, a broader and shorter signal is observed.

To clearly demonstrate these principles, we consider a hypothetical window function with a simple linear chirp in the $r-t$ plane, as illustrated in Fig. 4. Along with the window functions, we provide a representative sampling of the trajectories. The observable signals for the three cases—positive, negative, and no chirp—are also illustrated. Note, the signal is the convolution of the window function with the trajectory which operationally corresponds to flipping the time axis of the window function then evaluating the overlap integral under the window translated in time. The positively chirped window produces a shorter signal for the precollision resonance, where the group velocity of the swarm is positive, and a taller signal for the postcollision resonance where the group velocity of the swarm is negative. The inverse is true for the negatively chirped window.

Quite clearly, in the case of the chosen resonances at 393 and 398 nm, the effect of linear chirp in the pulse is less transparent, since the window function splits into a pair with oppositely chirped profiles (see Fig. 3). However, the spatial separation between the pair of windows implies that they will contribute to the signal at different times, with different intensities, producing a predictable overall signal as the sum of contributions from each window. We show the simulated

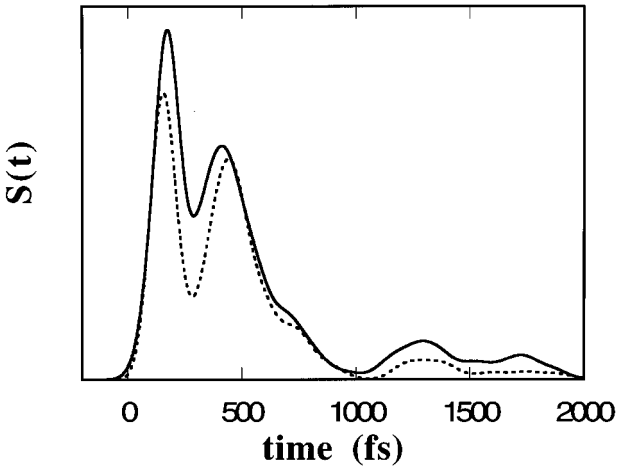

FIG. 5. The effect of probe chirp on the observable signal. The illustrated case is for an unchirped pump pulse, probed at 398 nm; dotted line, negatively chirped pulse (illustrated in Fig. 3); solid line, positively chirped pulse (mirror image of Fig. 3).

signal for the 398 nm resonance in Fig. 5, which was obtained using the pulse chirp and window functions shown in Figs. 3(a) and 3(b), and their mirror images. Note, in addition to the effect on relative heights of the signals arising from the two different resonances, the time separation between them is also changed. The latter is the result of the temporal asymmetry of the window function, the height of which is inversely proportional to the derivative of the difference potential according to Eq. (2).

Case (c): Chirped pump, unchirped probe

The effect of chirping the pump pulse is treated by presorting the trajectory ensemble. Thus, the trajectories are time ordered by their initial energies, using the slope of the pump chirp to determine the delay, Δt_0, between launching of trajectories,

$$\Delta t_0 = \pm \alpha [\Delta V_{A-X}(R_0) - \hbar \omega_0]. \tag{13}$$

Here, α has the same definition as in Eq. (9), the difference potential in this case corresponds to that of $I_2(A)-I_2(X)$, and $\hbar\omega_0$ is the central energy of the pump laser. The generation of the signal from the presorted trajectories is then accomplished by a single convolution over the probe pulse, i.e., as in Eq. (9) however, without the convolution over $P(t)$. In Fig. 6 we show the sorted trajectories for both positive and negative pump chirps, in each case in the inset we show magnification of the time origin. The slope of R_0 vs t_0 in the inset is the result of the monotonic nature of the difference potential. Here, we assume a chirped width for the pump pulse of FWHM=120 fs.

It should be obvious in Fig. 6 that in the case of the negatively chirped pulse the postcollision spread of the trajectory ensemble is smaller than in the case of the positively chirped pulse. This fact is illustrated in the phase portraits shown in Fig. 7, where the instantaneous $p-q$ distributions are shown for time delays of 200 fs and 398 fs, corresponding to the distributions under the precollision and postcollision resonances. The simulated signals for the two different pump chirps using an unchirped probe pulse of 41 fs is illustrated in Fig. 8. Quite clearly, the negatively chirped pulse focuses the recoiling packet more tightly than the positively chirped pump pulse, which is exhibited by the larger intensity in the signal arising from the postcollision resonance. The system memory of the pump chirp therefore outlasts the collision with the cage. In effect, the coherence in the bond remaking dynamics is being controlled by the shaped pump pulse.

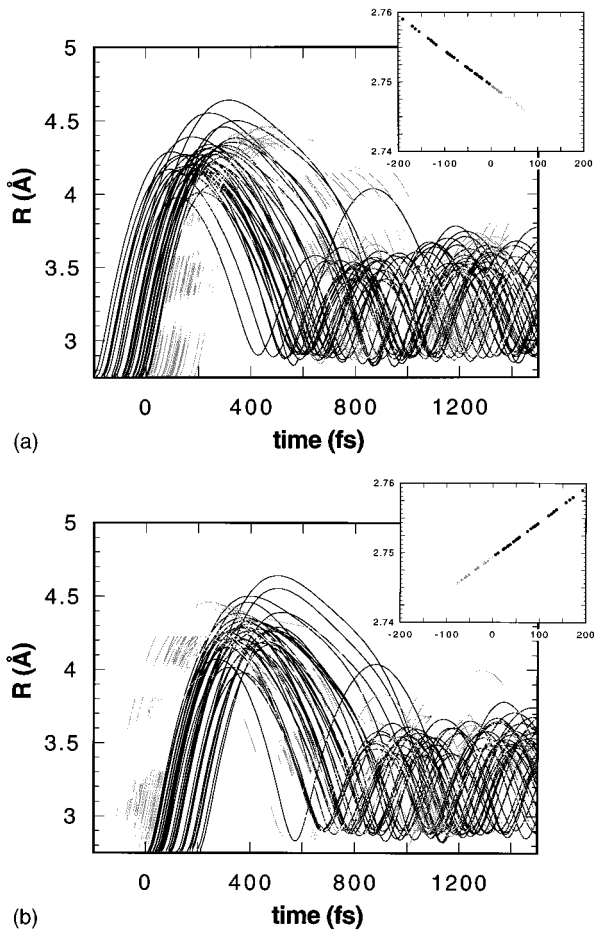

FIG. 6. Simulation of pump chirp. The trajectories are sorted according to their initial energies using the chirp coefficient α; (a) positively chirped pump, (b) negatively chirped pump. The insets show a magnification of the origin, which shows a slope in R_0 vs t_0, namely the initial separation of the I_2 bond length vs launch time of the trajectory (shorter internuclear distance corresponds to higher photon energy).

DISCUSSION

Seldom are pulse profiles carefully analyzed in ultrafast pump–probe studies. The usual practice is to operate with the shortest possible pulses, with various experimental criteria used to approach the transform limit. With the case study presented above, it is quite clear that for detailed interpretations of observables, the profiles of laser pulses used should be known. Chirped pulses can have profound effects on both preparation of a dynamical system and its interrogation;

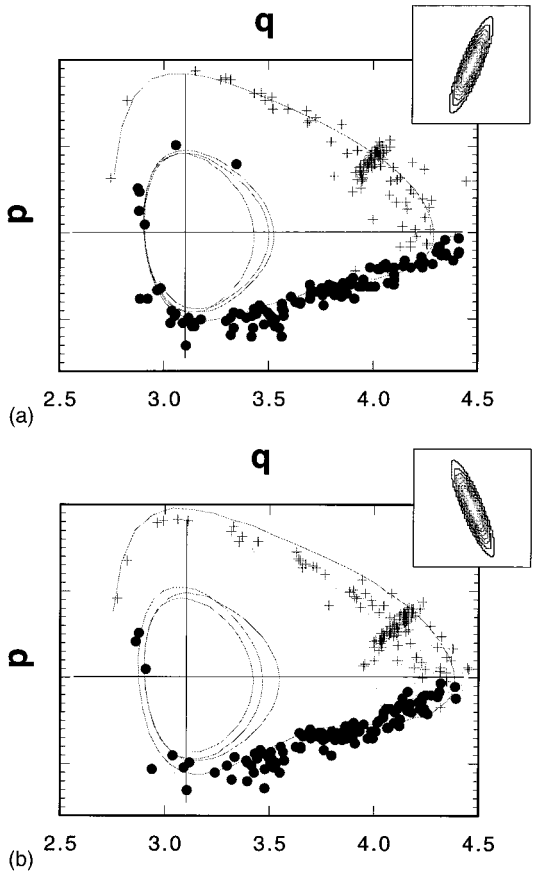

FIG. 7. Snapshots of the trajectory ensemble in phase space are shown, taken at the precollision resonance (+) and the postcollision resonance (●) are shown; (a) positively chirped pump, (b) negatively chirped pump. The negatively chirped pulse produces a tighter distribution at the postcollision resonance.

moreover, they can be used to extract subtle details about the system dynamics. These considerations were clearly illustrated in the model system considered in this paper. Prior to generalizing the results obtained, it is important to point the most severe approximation made in the treatment; the assumption that a one dimensional difference potential can be used for inversion of trajectories to observable signal. This is tantamount to the assumption that the guest–host interactions are identical in all electronic states. While in the particular case considered, the treatment has proven to be quite realistic, in general this should not hold, and a proper simulation of spectra will require evaluation of excited state energetics while simulating dynamics on a prepared state. It is also this approximation that makes the interpretation of the effect of the probe chirp on observables quite transparent, as we discuss below.

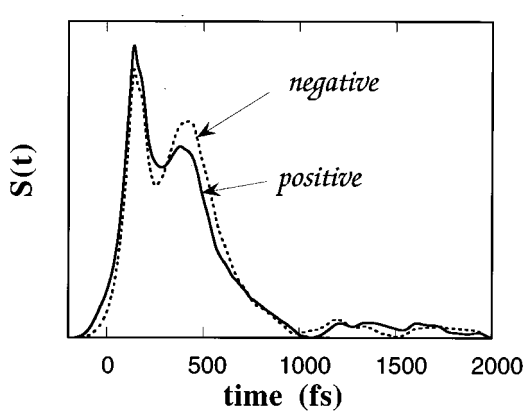

FIG. 8. The effect of pump chirp on the observable signal. The illustrated case is for chirped pump and unchirped probe [Fig. 1(a)] pulses. The pump chirps correspond to those of Fig. 6.

Probing with a chirped pulse corresponds to monitoring the evolving dynamics, or the traveling wave packet, through a window skewed in the $r-t$ plane. Skewing in turn corresponds to velocity, and therefore yields a traveling window function. Accordingly, the observable signal will be subject to a Doppler effect, namely the signal will be compacted when the window and wave packet are counterpropagating; and will be spread in time where they travel in the same direction. This effect emerges most clearly in the present example, which is limited to monitoring the single bounce of the I_2 wave packet from the Kr cage. In the outgoing wave the packet has positive velocity, and during its recoil it has a negative velocity. Accordingly, positively chirped windows sharpen the recoil resonance while negatively chirped windows do the opposite, as clearly illustrated in Fig. 4. In translating this to the pulse chirp, it should be recognized that the window function is a transformation of the probe pulse via the difference potential of the transition. Thus, a pulse chirped positively (in $\omega-t$ plane), will produce a positively chirped window function where the difference potential is positive and a negatively chirped window function where the difference potential is negative. In the case of double valued difference potentials, the window function contains both chirps as illustrated in Fig. 3. Nevertheless, the observable signal will be quite sensitive to the probe chirp, as illustrated in Fig. 5. Thus, in principle, by varying the chirp in the probe pulse it is possible to detect the direction of motion of the packet if the gradients of the difference potentials are known. Where the direction of motion of the packet is known, as in the present example, the effect of the probe chirp is useful in characterizing the difference potential. Note, it was also demonstrated that as long as flux is conserved the area under a given resonance is inversely proportional to the magnitude of the instantaneous group velocity of the packet. It should therefore be clear, that in the case where the resonance can be located in coordinate space, the pump–probe experiment with chirped pulses yields a simultaneous measure of the instantaneous position and momentum of the packet, $(q,\mathbf{p};t)$, therefore uniquely characterizes the underlying equations of motion.

In generalizing these considerations to multidimensional spectral inversions, it is important to note that the chirped window moves along the gradient of the difference potential of the probe transition, while the trajectories evolve along the gradient of the particular potential energy surface prepared by the pump pulse. It is possible to conceive situations where these two coordinates are orthogonal, and therefore the probe chirp will have minimal observable effect on the

detected signal. Even in the case of the one dimensional analysis, it is important to note that the ω–t distribution of the laser pulse is significantly distorted by the difference potential gradient, as clearly illustrated by the 398 nm probe case. In most cases, the many-body difference potentials are not known initially, especially so, where large amplitude motions away from stationary points on the various surfaces are probed. The common situation will call for iteration between experiment and simulation with chirped pulses to refine initial guesses of not only the surface over which the dynamics evolves, but also the terminal state used in the probe transition.

The observed effect of the pump chirp has far reaching implications. That a negatively chirped pulse will yield a more tightly focused packet on the recoil, is understandable in one dimensional anharmonic potentials; the trajectories launched at higher energy have longer to travel, and therefore will catch-up with the lower energy trajectories if started earlier. However, in the case under consideration—the dynamics of dissociation, collision with the wall, recoil, and recombination—highly nonlinear dynamics of many-body interactions is involved, as previously elaborated. In fact, it has clearly been argued previously that the long lasting coherences in this system, which survive extensive energy relaxation, are mainly controlled by the first collision of the wave packet with the lattice wall.[18] The elasticity of the cage has been one criterion to characterize the many-body response of the host to the impact of first collision. In that sense, Kr is significantly less elastic than Ar, which is manifested in the significantly reduced coherences in the recombined molecule.[17,18] Nevertheless, we clearly see that the system retains memory of its initial preparation. Experimentally, this will be clearly manifested by observing a sharper, and therefore higher, peak in the postcollision resonance, as illustrated in Fig. 8. A measure of the duration of this memory is the extent of coherence maintained in the postcollision dynamics, which experimentally is assessed by the depth of modulation in the observable signal during the vibrational relaxation of the newly formed molecule. We consider this in Fig. 9, by simulating the observable signal for a window situated at a shorter internuclear separation, for a probe pulse at 366 nm. It can be seen there that for the length of the simulation of 2 ps, the dynamics remains more coherent in the case of initial preparation by a negatively chirped pulse. This is quite significant in that it implies long lasting controllability in this system.

In considering the extent of memory in this particular system, it should be borne in mind that we have not carried out any exploration of pulse width, chirp or energy dependence, parameters that should be optimized for observing maximal control. The specific set of parameters we have chosen—a pump wavelength of 786 nm, with a chirp broadened width of 120 fs—were strictly based on parameters of an experimental system. Nevertheless, it is clear that when a packet is created with launch times linearly dependent on the potential energy along the I–I coordinate, then the system will remember this initial condition for chemically significant time scales. It is important to consider the extent of

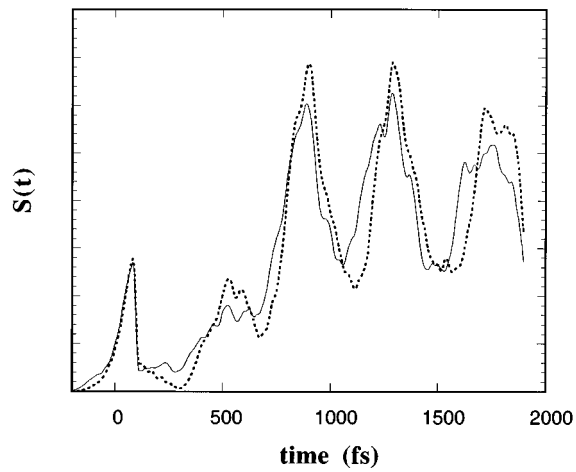

FIG. 9. Memory of the dynamics. When probed at 366 nm, the dynamics after recombination can be followed. For the duration of the simulation of 2 ps, the population prepared by the negatively chirped pulse (dotted line) remains more coherent than that prepared with positively chirped pump pulse (solid line) as evidenced by the deeper modulation of the observable signal.

control on the initial preparation. We again note that in our simulations we have used identical I–Kr potentials for both X and A states of I_2. This allows the preservation of the pump chirp in its transformation from frequency–time, to coordinate–time space. This was illustrated in Fig. 6. The control in the preparation of the initial distribution in phase space clearly depends on the mapping of the ground state thermal distribution onto the excited state with the radiation field. Given strong differences in forces along several guest–host coordinates between these two surfaces, the chirp of the pump pulse will be scrambled when transformed to coordinate space. Given the fact that the prepared coordinate space distribution plays the major role in determining the coherence of the evolving dynamics,[17,18] it is important to distinguish in controllability two separate aspects that come to play in the case of real systems; the controllability of preparation, and controllability given an initial preparation. The second of these was demonstrated here. The first hinges on the assumption that the I_2–Kr interactions are not significantly different in the X and A states in the excitation range considered. While this can be defended in part given the fact that the steep repulsive wall of the A state is accessed initially, where the dominant force is along the I–I coordinate, and in part from the knowledge that the $A \rightarrow X$ transition in Kr yields a structured emission spectrum, it nevertheless is an assumption which has not been fully quantified.

CONCLUSIONS

We have presented an analysis of pump–probe measurements with linearly chirped pulses as applied to condensed phase chemical dynamics. The system considered, photodissociation and cage induced recombination of I_2 in solid Kr, and the laser parameters used, were chosen with specific experiments in mind. The entire analysis was carried out by classical simulations, using a scaled temperature to mimic

the quantum distribution of the initial state. The most convincing justification of this approach is its success in previous treatments of this system.[16–18] Various semiclassical treatments of this system have also been considered recently.[32]

We have shown that the chirp of the probe pulse can be used as a vectorial diagnostic of the momentum of the evolving wave packet. A chirped probe pulse can be regarded as a window function traveling along the gradient of the difference potential of the probe transition. The relative velocity between the traveling window and the traveling wave packet determines the shape of the observable signal. Thus, studies with characterized pulse shapes add another dimension to the analysis of the underlying many-body interactions.

We have also shown that the system retains memory of its initial preparation. When the bond is broken with a negatively chirped pulse, it is remade with significantly more coherence than in the case of preparation with a positively chirped pulse, and this memory lasts even after vibrational relaxation in the newly made molecule. Despite the highly nonlinear dynamics that characterizes this process, the system is in effect controllable—a result which was not obvious prior to this treatment. In effect, it has been demonstrated that coherent control of chemistry in condensed media is possible.

Finally, we mention that the results obtained here are in qualitative agreement with preliminary experiments on this system, which were first executed in a collaboration with Kohler and Wilson of the UCSD.

ACKNOWLEDGMENTS

This research was supported under a grant from the U.S. Air Force Office of Scientific Research AFOSRF49620-1-0251. Stimulating discussions with C. C. Martens, K. R. Wilson, M. Ovchinnikov, Z. Li, M. Messina, J. Che, B. Kohler, and N. Schwentner at different stages of this project, are acknowledged with delight.

[1] D. J. Tannor and S. A. Rice, Adv. Chem. Phys. **70**, 442 (1988).
[2] S. A. Rice, Science **258**, 412 (1992).
[3] (a) D. Neuhauser and H. Rabitz, Acc. Chem. Res. **26**, 496 (1993); (b) H. Rabitz and S. Shi, Adv. Mol. Vib. Coll. Dyn. **1A**, 187 (1991).
[4] W. S. Warren, H. Rabitz, and M. Dahleh, Science **259**, 1581 (1993).
[5] M. Shapiro and P. Brumer, Int. Rev. Chem. **13**, 187 (1994).
[6] B. Kohler, J. Krause, F. Raksi, K. R. Wilson, R. M. Whitnell, V. V. Yakovlev, and Y. Yan, Acc. Chem. Res. **28**, 133 (1995).
[7] A. M. Weiner, D. E. Leaird, G. P. Wiederrecht, and K. A. Nelson, Science **247**, 1317 (1990).
[8] S. Chelkowski, A. Bandrauk, and P. B. Corkum, Phys. Rev. Lett. **65**, 2355 (1990).
[9] R. S. Judson, K. K. Lehmann, H. Rabitz, and W. S. Warren, J. Mol. Struct. **223**, 425 (1990).
[10] J. A. Cina and R. A. Harris, J. Chem. Phys. **100**, 2531 (1994).
[11] S. M. Park, S. P. Lu, and R. J. Gordon, J. Chem. Phys. **94**, 8622 (1991).
[12] M. Sugawara and Y. Fujimura, J. Chem. Phys. **100**, 5646 (1994).
[13] J. L. Herek, A. Materny, and A. H. Zewail, Chem. Phys. Lett. **228**, 15 (1994).
[14] B. Kohler, V. V. Yakovlev, J. Che, J. L. Krause, M. Messina, K. R. Wilson, N. Schwentner, R. M. Whitnell, and Y. J. Yan, Phys. Rev. Lett. **74**, 3360 (1995).
[15] J. Paye, IEEE J. Quantum Electron. **28**, 2262 (1992).
[16] R. Zadoyan, Z. Li, P. Ashjian, C. C. Martens, and V. A. Apkarian, Chem. Phys. Lett. **218**, 504 (1994).
[17] R. Zadoyan, Z. Li, C. C. Martens, and V. A. Apkarian, J. Chem. Phys. **101**, 6648 (1994).
[18] Z. Li, R. Zadoyan, V. A. Apkarian, and C. C. Martens, J. Phys. Chem. **99**, 7453 (1995).
[19] R. Zadoyan, B. Kohler, K. R. Wilson, and V. A. Apkarian (in preparation). For a preliminary report, see V. A. Apkarian, in *Femtochemistry* (World Scientific, Singapore, 1996).
[20] X. N. Zheng, S. I. Fei, M. C. Heaven, and J. Tellinghuisen, J. Mol. Spectrosc. **149**, 399 (1991).
[21] J. Franck, Trans. Faraday Soc. **21**, 536 (1925).
[22] (a) G. Herzberg, *Molecular Spectra and Molecular Structure. I. Spectra of Diatomic Molecules*, 2nd ed. (Van Nostrand, Princeton, 1950), pp. 391–394; (b) J. G. Winan and E. C. G. Stueckelberg, Proc. Natl. Acad. Sci. USA **14**, 867 (1928); (c) G. E. Gibson and N. S. Bayliss, Phys. Rev. **44**, 188 (1933); (d) E. J. Heller, J. Chem. Phys. **68**, 2066 (1978).
[23] See, for example, M. E. Fajardo and V. A. Apkarian, J. Chem. Phys. **89**, 4102 (1988).
[24] R. G. Gordon, Adv. Magn. Reson. **3**, 1 (1968).
[25] E. J. Heller, J. Chem. Phys. **62**, 1544 (1975).
[26] L. E. Fried and S. Mukamel, J. Chem. Phys. **93**, 3063 (1990).
[27] J. P. Bergsma, P. H. Berens, K. R. Wilson, D. R. Fredkin, and E. J. Heller, J. Phys. Chem. **88**, 612 (1984).
[28] M. P. Allen and D. J. Tildesley, *Computer Simulation of Liquids* (Clarendon, Oxford, 1987).
[29] J. Tellinghuisen, Can. J. Phys. **62**, 1933 (1984).
[30] J. Almy and V. A. Apkariah (in preparation).
[31] R. Zadoyan, M. Sterling, and V. A. Apkarian, Faraday Research Article, Faraday Transactions (in press).
[32] J. Che, M. Messina, K. R. Wilson, V. A. Apkarian, Z. Li, C. C. Martens, R. Zadoyan, and Y. J. Yan, J. Phys. Chem. (submitted).